IR Spectroscopy of α- and β-Protonated Pyrrole via Argon Complex Photodissociation

ARTICLE *in* THE JOURNAL OF PHYSICAL CHEMISTRY A · SEPTEMBER 2012

Impact Factor: 2.69 · DOI: 10.1021/jp307631n · Source: PubMed

THE JOURNAL OF PHYSICAL CHEMISTRY A

Article

pubs.acs.org/JPCA

IR Spectroscopy of α- and β-Protonated Pyrrole via Argon Complex Photodissociation

J. D. Mosley, A. M. Ricks, P. v. R. Schleyer, J. I. Wu, and M. A. Duncan*

Department of Chemistry, University of Georgia, Athens, Georgia 30602-2556, United States

Supporting Information

ABSTRACT: Protonated pyrrole cations are produced in a pulsed discharge/supersonic expansion source, mass-selected in a time-of-flight spectrometer, and studied with infrared photodissociation spectroscopy. Vibrational spectra in both the fingerprint and C−H/N−H stretching regions are obtained using the method of tagging with argon. Sharp vibrational structure is compared to IR spectra predicted by theory for the possible α-, β-, and N-protonated structures. The spectral differences among these isomers are much larger than the frequency shifts due to argon attachment at alternative sites. Though α-protonation predominates thermodynamically, the kinetically favored β-protonated species is also observed for the first time (in 3−4 times lower abundance under the conditions employed here). Theoretical investigations attribute the greater stability of α-protonated pyrrole to topological charge stabilization, rather than merely to the greater number of resonance contributors. The far-IR pattern of protonated pyrrole does not match the interstellar UIR bands.

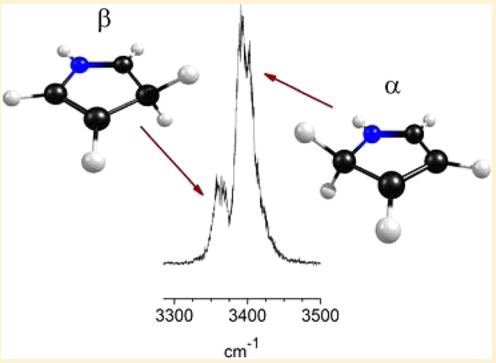

INTRODUCTION

Protonation and proton transfer, arguably the most fundamental chemical reactions, also are crucial in biology, astronomy, and physics.[1,2] The structures of the proton binding sites of molecules and the energetics involved provide keys to proton transfer and other intermediate steps along reaction pathways. Protonated organic molecules are important reaction intermediates,[3] and they can also serve as prototypes for processes such as electrophilic aromatic substitution. Though energetic and kinetic data on protonated species are available from mass spectrometric studies,[4] elucidation of the structures of ions in the gas phase (the topic of this paper) is extremely challenging[5] and requires new experimental approaches.

Pertinent, but less refined, information about the nature of persistent protonated ions in condensed phases was given by, e.g., Olah's extensive investigations in superacid media, typically using NMR and IR spectroscopy.[3] A substantial number of X-ray structures also are now available.[6,7] These extensive data show that aromatic rings are typically protonated at σ rather than at π sites.[8−11] Protonated benzene is the classic example of such arenium ions.[9−11] Higher quality infrared spectra without the interference of solvent or counterions have been obtained by recent gas phase experiments on mass-selected ions; these confirm the prior experimental and theoretical conclusions about the structure of the benzenium ion.[12−15] Such gas phase IR studies have been extended recently to other protonated arenes, such as toluene,[15] naphthalene,[16,17] or larger polycyclic aromatics.[18] Substituted aromatic rings offer multiple protonation sites, the competition among which depends on their intrinsic stability in the gas phase.[19−26] In these gas phase experiments, the complicating effects in solution, such as the interaction with the counterion and the solvation environment, are eliminated.

The present report employs gas phase methods, supported by theoretical computations, to investigate the protonation of pyrrole, a simple aromatic nitrogen heterocycle.[27−38] The gas phase protonation of related heterocyclic compounds has also been investigated previously with ion reaction kinetics and infrared spectroscopy. Protonation of furan and thiophene at sites other than at O or S were preferred despite the availability of in-plane heteroatom lone pairs.[26] In other illustrative ion infrared spectroscopy experiments, Dopfer and co-workers' study of the protonation of phenol also indicated the presence of multiple protonation sites, both on the OH group and on the ortho/para sites of the aromatic ring.[19] Likewise, when aniline was complexed with neutral ligands, protonation at the amino group N-site competed with sites on the phenyl ring.[20] The nitrogen atoms of heterocycles like imidazole and 1-azapyrene are the primary protonation sites.[20−23,25]

Pyrrole has three possible protonation sites, at the nitrogen as well as the two nonequivalent carbons of the five-member ring. Though electrophilic substitution of pyrrole in solution is well-known to occur primarily at the α position, its α/β branching ratio is smaller than other five-membered ring heterocycles like furan and thiophene, and there is considerable variation with different solvent systems.[27,28] Gas phase reaction studies result in similar findings.[29−33] Extensive computational investigations of the relative energies of different intermediates

Received: August 1, 2012
Revised: September 8, 2012
Published: September 11, 2012

dx.doi.org/10.1021/jp307631n | J. Phys. Chem. A 2012, 116, 9689−9695

indicate that the α-protonated isomer has the lowest energy.[29,32,35−37] The conventional interpretation attributes this α preference to the greater number of resonance contributors.[28] We propose a better-founded explanation here. In contrast, note that molecular electrostatic potentials and the greater charge density predict greater reactivity at the β position.[34−38] We now provide experimental evidence for this as well.

Dopfer and co-workers carried out the most closely related prior gas phase spectroscopy of protonated pyrrole by using IR multiphoton dissociation spectroscopy (IR-MPD) with a free electron laser in the fingerprint region (900−1800 cm^{-1}).[26] From the comparison of the single broad (~80 cm^{-1} fwhm) band measured at 1426 cm^{-1} with spectra predicted by theory, these investigators concluded that the α-protonated species was the only isomer present.[26] Here, we obtain higher resolution data using single photon infrared photodissociation spectroscopy (IR-PD) and extend the spectrum of protonated pyrrole over a broader infrared region (800−4500 cm^{-1}). This enables the identification of both the α- and β-protonated structures, the latter for the first time.

EXPERIMENTAL DETAILS

Protonated pyrrole is produced in a coaxial ring discharge/supersonic expansion source described previously.[15,17] The expansion consists of the vapor of pyrrole at 25 °C seeded in a gas mixture of about 10% H_2 in Ar. After generation and cooling, the cations are pulse extracted into a reflectron time-of-flight mass spectrometer located in a differentially pumped chamber. This instrument is used for selected-ion photodissociation spectroscopy as described previously.[39] Because the density of ions after mass selection is far too low for absorption spectroscopy, we employ photodissociation to detect vibrational resonances. As IR photons on resonance with vibrational fundamentals generally do not have enough energy to break covalent bonds, argon tagging is employed to obtain these spectra.[39−44] The ion of interest is selected by its flight time using pulsed deflection plates located in the first flight tube. Photodissociation occurs in the turning region of the reflectron, where the selected ion packet overlaps in time and space with the output of a pulsed, tunable infrared optical parametric oscillator/amplifier (OPO/OPA) laser system (LaserVision). The OPO/OPA system is pumped with the output of an Nd:YAG laser (Spectra-Physics PRO-230), providing tunable radiation from 600−4000 cm^{-1} with a bandwidth of about 1.0 cm^{-1}.[45,46] Absorption on resonance with the molecular ion causes elimination of argon. The resulting fragment ion is separated from the parent ion by its flight time in a second drift tube. This fragment ion signal is collected as a function of the laser energy using a digital oscilloscope (LeCroy WaveRunner).

Computations at the DFT/B3LYP and MP2 levels of theory using the 6-311++G(2d,2p) basis set are employed to investigate the structures of different isomers resulting from protonation at different sites and to predict their harmonic vibrational spectra. These computations are done with and without the attached argon to investigate its influence on these spectra. We also investigate different binding sites for the argon atom. All of these studies were performed with the GAMESS program.[47] The harmonic vibrational frequency scaling factors employed (0.9813 in the 1000−1800 cm^{-1} fingerprint region and 0.9629 in the 2800−3600 cm^{-1} region) were derived from calculated frequencies for neutral pyrrole at the same level of theory by comparison to the known experimental values.[48] The energetics of other selected species were also investigated at the B2PLYP/6-311+G(2d,2p) level. NICS computations were performed at the PW91/IGLOII level.

RESULTS AND DISCUSSION

The IR-PD spectrum for argon-tagged protonated pyrrole in the fingerprint region of the IR (1000−1800 cm^{-1}) is shown in Figure 1. The previous IR-MPD spectroscopy by Dopfer and co-workers found only one broad resonance in this region.[26] In contrast, our argon tagging spectrum reveals several relatively sharp bands. However, the extremely weak signal in this region (attributed to a low photodissociation efficiency) required extensive averaging. The additional details available in this spectrum were assigned by comparison with theoretical vibrational spectra computed at the DFT/B3LYP/6-311++G(2d,2p) level for α-, β-, and N-protonated structures both with and without argon tags. The performance of this level of DFT theory was validated for this purpose in our previous work.[15,17] The relative energies for the α-, β-, and N-protonated structures, with and without argon, at both B3LYP- and MP2-optimized levels, are presented in Table 1. Consistent with previous findings, the α position is the best protonation site; β-

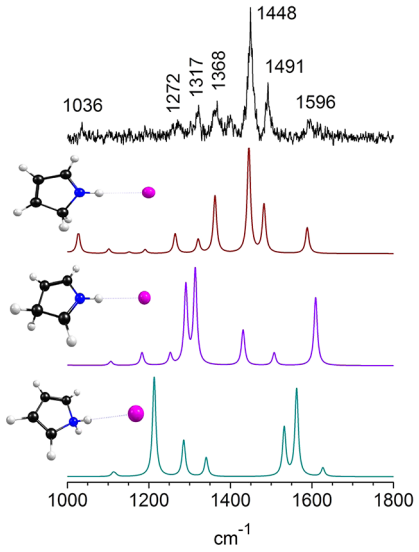

Figure 1. IR-PD spectrum of protonated pyrrole tagged with argon in the 1000−1800 cm^{-1} region compared with computations performed at the B3LYP/6-311++G(2d,2p) level of theory.

Table 1. Computed Relative Energies among Structures with and without Ar (Relative to the Lowest Energy Structure, in kcal/mol)

isomer	B3LYP[a]	B2PLYP-D[b]	MP2[a]
α-pyrrole-H^+	0.0	0.0	0.0
β-pyrrole-H^+	5.3	4.8	4.3
N-pyrrole-H^+	20.8		17.9
α-pyrrole-H^+-Ar	0.0		0.0
β-pyrrole-H^+-Ar	5.2		4.2
N-pyrrole-H^+-Ar	20.5		17.4

[a]Using the 6-311++G(2d,2p) basis set; ZPE corrected. [b]Using the 6-311+G(2d,2p) basis set; no ZPE. The relative energy of the $\alpha \rightarrow \beta$ TS is 22.8 kcal/mol at this level.

dx.doi.org/10.1021/jp307631n | J. Phys. Chem. A 2012, 116, 9689−9695

protonation is ~5−6 kcal/mol higher in energy. N-protonation is quite unfavorable. Argon attachment is most favorable at the H−N position of each of the α-, β-, and N-protonated isomers. However, Figure 2 shows that three other argon binding sites

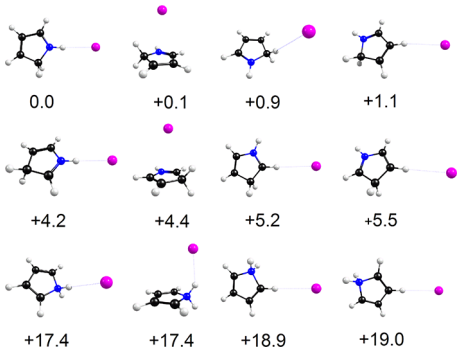

Figure 2. Structures and energetics of possible argon isomers of protonated pyrrole at the MP2/6-311++G(2d,2p) level. Energies (kcal/mol, ZPE corrected) are relative to the most stable "Ar-on-HN" isomer of α-protonated pyrrole.

are also close in energy (see the Supporting Information for full details). Although argon attachment above the ring is the most stable binding site for protonated benzene,[49] such argon positions are slightly less favorable for protonated pyrroles. However, as shown in Figure 2, the energy differences for different argon isomers are quite small, and the presence of argon does not affect the relative energetics of the three different protonation structures in any significant way. Table 2 shows the vibrational frequencies computed for the different isomers after appropriate scaling and the shift on each vibration induced by the presence of argon (bound in the H−N position). The observed vibrational bands are tabulated here for comparison with these computed values.

In addition to the experimental spectrum in the fingerprint region, Figure 1 shows the vibrational spectra predicted by for each of the three "Ar-on-HN" protonated structures. The corresponding spectra for other argon isomers are essentially the same (see the Supporting Information). The most intense peak at 1448 cm^{-1} is assigned to a ring carbon stretch/in-plane hydrogen bend, with significant participation of the N−H group. This peak has a line width (fwhm) of ~14 cm^{-1} and corresponds well with the previously observed IR-MPD transition at 1426 cm^{-1}.[26] For comparison, the frequency of the corresponding υ_{19} vibration in neutral pyrrole is 1518.5 cm^{-1}.[48] Similarly, the relatively strong band at 1491 cm^{-1}, also assigned to a ring carbon stretch/in-plane hydrogen bending motion, corresponds most closely with the υ_{19} vibration in neutral pyrrole; the single strong band in the neutral splits into a doublet in the lower symmetry ion. The charge is responsible for the slightly lower frequency in the ion than in the neutral. As documented for protonated benzene,[12,13,15] protonation decreases the aromaticity and the rigidity of the system. Other significant features include the ring breathing mode at 1036 cm^{-1}, the CH_2 scissors motion at 1368 cm^{-1}, and the asymmetric carbon ring stretching mode at 1596 cm^{-1}. The latter two modes correspond to those for protonated benzene at 1239 and 1607 cm^{-1}.[15] The scissors motion occurs at a significantly higher frequency for protonated pyrrole, and the carbon ring vibrations are about the same for the two systems. Although the vibrations in this region are very similar for α- and β-protonated isomers, their intensity profiles (and that for the

Table 2. IR-PD Bands of Protonated Pyrrole Compared to the Predictions of Theory at the B3LYP/6-311++G(2d,2p) Level[a]

exp (cm^{-1})	theory (int)	Δν(Ar)	assignment (isomer)
1036	1042 (15.9)	+0.1	ring breathing (α-prot)
1272	1270 (15.1)	−14.1	CH_2 wag ip (α-prot)
1317	1339 (8.41)	+0.2	β-CH/β-CH asym wag ip (α-prot)
1368	1372 (42.0)	−5.1	CH_2 scissors (α-prot)
1448	1466 (95.2)	+4.7	NH/α-CH asym wag ip (α-prot)
1491	1502 (30.2)	+3.8	sym ring stretch (α-prot)
1596	1609 (19.9)	+2.0	asym ring stretch (α-prot)
2892	2910 (40.5)	+0.7	sym CH_2 stretch (β-prot)
2917	2929 (21.6)	−3.0	sym CH_2 stretch (α-prot)
2917	2927 (16.7)	+0.9	asym CH_2 stretch (β-prot)
2948	2961 (10.8)	−3.7	asym CH_2 stretch (α-prot)
3080	3120 (28.5)	−0.3	α-C−H stretch (β-prot)
3095	3107 (5.7)	+0.7	α-C−H stretch (α-prot)
3095	3136 (16.1)	−0.3	asym CH−CH stretch (β-prot)
3114	3120 (12.6)	+0.6	asym CH−CH stretch (α-prot)
3114	3156 (10.7)	+0.0	sym CH−CH stretch (β-prot)
3135	3141 (15.0)	+0.0	sym CH−CH stretch (α-prot)
3186		unassigned	
3248		unassigned	
3364	3372 (418)	−54.8	N−H stretch (β-prot)
3396	3418 (461)	−47.0	N−H stretch (α-prot)

[a]Vibrations are scaled by a factor of 0.9813 in the fingerprint region (1000−1800 cm^{-1}) and 0.9629 in the higher frequency region (2800−3600 cm^{-1}) for comparison to the experiment. The computed shifts in vibrational frequencies due to argon complexation (HN position) are given as Δν(Ar).

N-protonated species) are quite different. The computed band positions, and especially the profile of the α-protonated species, agree much better with the experiment than those of the other two structures. Hence, from only the spectrum in this wavelength region, it appears (misleadingly) that only the α-protonated species is present. This same (erroneous) conclusion was deduced by Dopfer and co-workers from their IR-MPD spectroscopy experiment.[26] However, it should be noted that the signal level in this region is relatively low, and bands from another isomer might be missed if it were present in low concentration.

Figure 3 shows the infrared spectrum of protonated pyrrole in the higher frequency region (2800−3600 cm^{-1}), where the greater IR laser power results in better signal levels. Three groups of bands are detected, a triplet near 2900 cm^{-1}, a quartet near 3100 cm^{-1}, and a doublet at 3364/3396 cm^{-1}. The second trace from the top of the figure shows the vibrational spectrum expected for the α-protonated structure with argon bound at its most favorable H−N site. It is immediately evident that the experimental spectrum has too many bands to be accounted for by this single species. Because the Figure 1 data suggested the presence of only the α-protonated structure, we first consider the possibility that the additional multiplets in Figure 3 might arise from argon attachment isomers. The lower traces in the figure therefore show the spectra predicted for the α-protonated structure having argon binding at the CH_2 and CH binding positions. However, as shown in Figure 3, the argon-induced frequency shifts in these vibrations are small. Argon has the greatest effect at its binding site; the N−H stretch is red-shifted substantially when argon binds here, but it

dx.doi.org/10.1021/jp307631n | J. Phys. Chem. A 2012, 116, 9689−9695

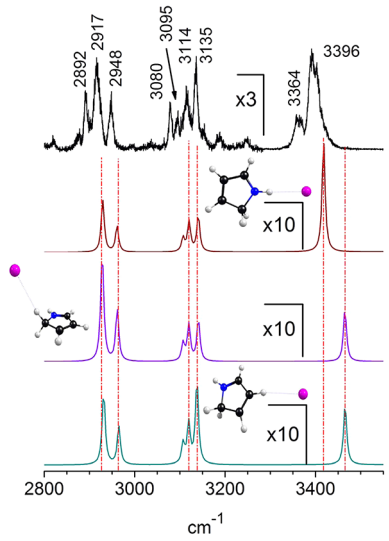

Figure 3. IR-PD spectrum of protonated pyrrole tagged with argon in the 2800−3600 cm^{-1} region compared to spectra predicted (DFT/B3LYP/6-311++G(2d,2p); scaled) for isomers with different argon binding sites.

has a higher frequency when argon binds at other positions. If argon binds on the CH_2 group, the doublet for the symmetric and asymmetric stretches should be red-shifted, but this does not happen. In short, the frequency shifts due to argon binding at different positions on the α-protonated isomer are too small to account for the additional peaks observed in the higher frequency region of the IR. We therefore investigate other protonation sites as the source of these multiplets.

Figure 4 shows the higher frequency region of the spectrum compared to spectra predicted for the three protonated minima, each now with argon in its most favorable H−N binding site. Two bands near 2900 cm^{-1} are expected for each of the α- and β-protonated isomers corresponding to the symmetric and asymmetric CH_2 stretches. Each isomer should also have three aromatic C−H stretches near 3100 cm^{-1}. As

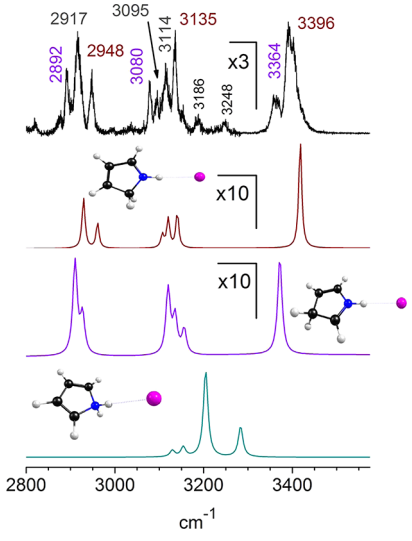

Figure 4. IR-PD spectrum of protonated pyrrole tagged with argon in the 2800−3600 cm^{-1} region compared with spectra predicted (DFT/B3LYP/6-311++G(2d,2p); scaled) for the α- (red) and β- (violet) and N-protonated (green) isomers.

shown, the number of bands detected experimentally in both frequency regions (top spectrum) clearly exceeds those attributable to a single isomer. However, a composite of bands from each of the α and β isomers accounts nicely for the multiplets observed. None of the band positions predicted by theory in this region are in perfect agreement with the experiment (Table 2); they are all slightly higher than measured. This is consistent with a small imperfection in the scaling factor used for the theory in this region. However, the relative positions of bands and their intensities indicate that a composite of both isomers can fit the observed pattern. Finally, in agreement with expectations and the computations, each of the α- and β-protonation structures should have a single strong N−H stretch at high frequency near 3400 cm^{-1}. In fact, two bands are observed, a more intense one at 3396 cm^{-1} and a weaker one at 3364 cm^{-1}. As shown in Figure 4, these two bands line up nicely with the predictions of theory for the α- and β-protonated structures, respectively. This is perhaps the most convincing evidence that both the α- and β-protonation structures are present. In contrast, there is no clear indication for the presence of any N-protonated isomer. This species should have strong symmetric and asymmetric NH_2 stretches near 3200 and 3300 cm^{-1}. There are two very weak bands near here, but the match with theory for their positions and splitting is not compelling. Theory predicts the N-protonated structure to be unfavorable energetically by about 20 kcal/mol (Table 2). Therefore, although there was no clear evidence for the β isomer in the lower frequency region of Figure 1 (or in previous work),[26] the data in the higher frequency region (Figure 3) indicate clearly that both the α- and β-protonated structures are present. Because the computed IR intensities for the N−H stretches are comparable for these two isomers (Table 2), and these bands overlap less than others, their intensities can be used to estimate the relative abundance of the two isomers. This comparison indicates that the α isomer is 3−4 times more abundant than the β species. In light of this, it is easy to understand why the β species was not detected in the lower frequency region spectrum shown in Figure 1 (as well as in the prior study).[26]

How is it that the β-protonated pyrrole isomer, despite being ∼5−6 kcal/mol higher in energy than the α, is produced, survives, and is detected in our experiment? Clearly, this is not expected if rapid equilibration over low barriers takes place, because then no discernible amount of the β isomer should remain. On the other hand, if the barriers to interconversion are high, the *kinetics* of the competing protonation reaction paths in the plasma (rather than the thermodynamics) would govern the relative amounts of the two isomers. These issues are complicated further because of our experimental conditions. At the moment of the pulsed discharge the temperature is highest, but it is not well-defined because of the different rates of excitation and collisional relaxation in the supersonic expansion and the short time period (microseconds) of interaction. Therefore, equilibrium between electronic and vibrational degrees of freedom is not expected.

We explored these alternatives by computing the barrier heights (without attached argon) for the circumambulatory proton transfer paths connecting each of the isomeric $C_4H_6N^+$ structures. Despite the caveat that DFT activation barriers may be too high,[50] the resulting DFT/B3LYP/6-311+G** data should at least be instructive. As shown in Figure 5, the barriers for $\alpha \rightarrow \beta$ (25.2 kcal/mol) or $\beta \rightarrow \alpha$ (19.4 kcal/mol) are both rather large, consistent with previous estimates.[32] The 25.2

dx.doi.org/10.1021/jp307631n | J. Phys. Chem. A 2012, 116, 9689−9695

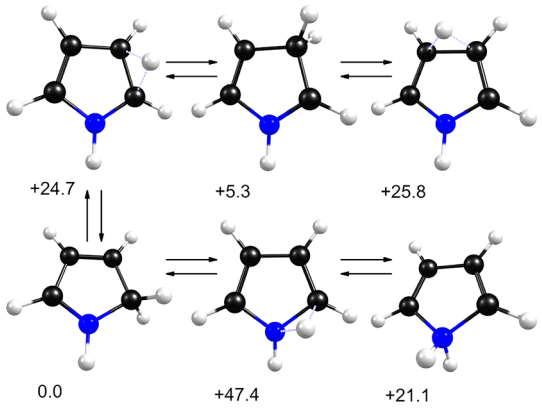

Figure 5. Structures and relative energies of sequential stationary points on the potential energy surface of protonated pyrrole computed at the DFT/B3LYP/6-311+G** level of theory. Structures with bridging protons are transition states. Energies (kcal/mol, ZPE corrected) are relative to the α-protonated global minimum.

kcal/mol value changes only slightly to 22.8 kcal/mol at the B2PLYP-D level. Consequently, the lack of full equilibration between the α and β isomers under our experimental conditions is understandable. Instead, our isomer ratio seems to reflect the formation (and survival) rates in the plasma. Related evidence indicates that the β position of pyrrole is more basic and has the higher electrostatic potential.[34−38] There is also experimental evidence that the β position may be more reactive.[34]

But why is protonation at the α position favored thermodynamically in pyrrole? Pyrrole protonation at the β position is kinetically favored on the basis of its atomic charges (more negative compared to the α position), but "electrostatic effects are not the sole factors involved in the interaction of a substrate with an electrophile."[34] The conventional explanation argues that the α isomer is favored due to the possibility of more resonance forms (as shown in Figure 6),[29,35] but there is a problem with this reasoning, as some of these forms may not be effective. Instead, the $\alpha > \beta$ site protonation preference for pyrrole (also of furan) is due to the effect of "topological charge

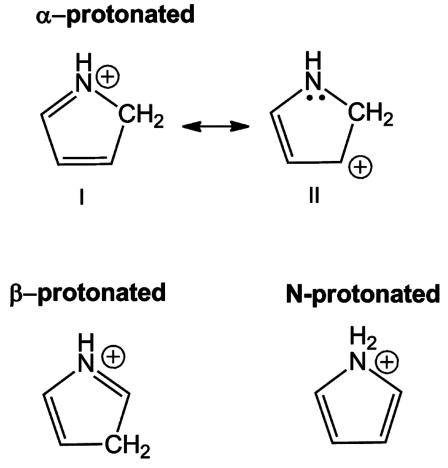

Figure 6. Natural resonance theory (NRT) analysis of the dominating resonance contributors for the α-, β-, and N-protonated pyrrole (at PW91/IGLOIII). Only contributors with >10% weights are shown. Unlike the β- and N-protonated pyrrole, α-protonated pyrrole has two major resonance contributors.

stabilization".[51] According to this principle, "heteroatoms prefer to be located at sites that conform to the pattern of relative electron densities determined by connectivity or topology in an isoelectronic, isostructural, homoatomic system called the uniform reference frame."[51b] For protonated pyrrole, cyclopentadiene is the uniform homoatomic isostructural reference frame. Hence, isoelectronic heteroatom replacement by the more electronegative N+ occurs preferentially at C1 (the terminus of the diene system) because the π charge densities are greater than those at C2. The same is true for butadiene; replacement of a C by N+ is preferred at the terminus C1, rather than at the C2 position.[51c] The topological charge stabilization effect is enhanced for protonated furan (because O is more electronegative than N) and explains why electrophilic substitution of furan gives almost exclusively α products. Hence, the α- vs β-protonated pyrrole energy difference is only 5.3 kcal/mol (computed at the B3LYP/6-311+G** +ZPE, favoring the α), but that of α- vs β-protonated furan preference is 11.8 kcal/mol. This striking difference cannot be explained by invoking the conventional explanation that the α-protonated isomers have more resonance forms, because both α-protonated pyrrole and furan have the same advantage.

Another misconception is that the protonation of pyrrole at any site eliminates its aromaticity completely. But this does not happen even when benzene is protonated.[12,13,15] As discussed below, the aromaticity and resonance stabilization of both α- and β-protonated pyrrole are about the same. Protonation at the N-site of pyrrole is unfavorable because it would reduce aromaticity to a much greater extent than protonation at the α or β sites. Computed nucleus independent chemical shift (NICS) values provide a convenient indicator for the aromaticity of these different isomers.[52,53] Dissected $NICS(0)_{\pi zz}$ data, computed at the ring centers (at the PW91/IGLOII level) document this well. $NICS_{\pi zz}$ is the most reliable NICS index for assessing π aromaticity, as it extracts the out-of-plane "zz" tensor component of the isotropic NICS and includes only the π molecular orbital contributions.[53] The benzene-like $NICS(0)_{\pi zz}$ value of neutral pyrrole (−32.8 ppm), compared to −35.6 ppm for benzene, confirms its aromaticity, and the −6.6 ppm value confirms the essential nonaromaticity of its N-protonated form. In contrast, both the α- (−13.3 ppm) and β-protonated (−13.1 ppm) isomers have larger, modestly aromatic, $NICS(0)_{\pi zz}$ values, but these are nearly the same and the α and β isomers cannot be differentiated on this basis. The CH_2 groups in α- and β-protonated pyrrole act as 2π electron donors and are involved hyperconjugatively with the four π electrons in the ring to sustain "6π electron" aromaticity (more so than in their isoelectronic prototype, cyclopentadiene).[54] But this effect is attenuated in N-protonated pyrrole; the isoelectronic NH_2^+ group hyperconjugates less effectively because the electrons are more tightly bound to the electronegative N. Although protonation of nitrogen lone pairs in heterorganic molecules usually is preferred, this is not the case when the lone pairs are involved in aromatic delocalization.

The infrared spectroscopy of small aromatic ions is highly interesting for interstellar chemistry. In particular, unassigned infrared emission bands (UIR's) seen in many interstellar environments are believed to be caused by polycyclic aromatic hydrocarbon (PAH) species or their ions.[55] These bands in the fingerprint region of the IR occur in the wavelength region shown here in Figure 1. Although many PAH neutral and ionized species have been investigated, until recently none of

dx.doi.org/10.1021/jp307631n | J. Phys. Chem. A 2012, 116, 9689−9695

their spectra were found to match the UIR patterns. However, new work by our group[15] and by Dopfer and co-workers[18] has shown that protonated PAH species match nicely with at least some of the major UIR bands (6.2, 7.7, and 8.6 μm; 1613, 1299, and 1163 cm^{-1}). On the basis of computed vibrational spectra, Hudgins and co-workers have suggested that nitrogen substituted aromatic rings provide potentially better matches to the UIR's,[56] but few of these ring systems have been investigated experimentally in the fingerprint region. The present work shows that protonated pyrrole lacks bands at the matching wavelengths indicated above and can therefore be excluded as a possible contributor to these UIR features.

CONCLUSIONS

The vibrational spectra of protonated pyrrole cations, produced in a pulsed discharge/supersonic nozzle source, were determined with photodissociation spectroscopy, both in the fingerprint and in high frequency infrared regions. The use of argon tagging produced spectra with better resolution and sensitivity over a larger frequency range than those obtained previously. While the vibrational patterns in the fingerprint region suggest (erroneously) the presence only of the more stable α-protonated isomer, the higher frequency region spectra show clearly that β-protonated pyrrole is present as well, even though it is computed to be 5−6 kcal/mol less stable than the α isomer. There is no clear evidence for N-protonation. Although multiple possible attachment sites complicate the argon tagging method (there are at least four argon positions in protonated pyrrole), their energy differences are small. The influence of different protonation sites on the vibrational spectra is much larger than that from different argon sites. Consequently, tagging does not interfere with the identification of the protonated pyrroles actually present. The activation barriers for interconversion of α- and β-protonated pyrrole isomers are computed to be quite high (>15 kcal/mol), consistent with the coexistence of both isomers under the experimental conditions. Although less stable, the β isomer evidently is formed kinetically during ion production in the plasma source. Computational investigations attribute the greater stability of α-pyrrole to topological charge stabilization. The far-IR spectrum of protonated pyrrole does not resemble the features observed in the unidentified interstellar UIR bands.

ASSOCIATED CONTENT

Supporting Information

The geometric and energetic parameters for the protonated pyrrole isomers and the isomers with argon attached at different positions, as well as the details of NICS computations. This material is available free of charge via the Internet at http://pubs.acs.org.

AUTHOR INFORMATION

Corresponding Author

*E-mail: maduncan@uga.edu.

Notes

The authors declare no competing financial interest.

ACKNOWLEDGMENTS

We gratefully acknowledge support from the National Science Foundation for this work, through Grants CHE-0956025 (M.A.D.) and CHE-1057466 (P.v.R.S.). We thank E.-U. Würthwein for discussions.

REFERENCES

(1) Bell, R. P. *The Proton in Chemistry*; Chapman & Hall: London, 1973.
(2) Hynes, J. T., Klinman, J. P., Limbach, H.-H., Schowen, R. L., Eds. *Hydrogen-Transfer Reactions*; Wiley-VCH Publishers: Weinheim, 2006.
(3) Olah, G. A.; Prakash, G. K. *Carbocation Chemistry*; Wiley: New York, 2004.
(4) Holmes, J. L.; Aubry, C.; Mayer, P. M. *Assigning Structures to Ions in Mass Spectrometry*; CRC Press: Boca Raton, FL, 2007.
(5) Baer, T.; Ng, C.-Y.; Powis, I. *The Structure, Energetics and Dynamics of Organic Ions*; John Wiley & Sons: Chichester, U.K., 1996.
(6) Laube, T. *Acc. Chem. Res.* **1995**, *28*, 399−405.
(7) Aue, D. H. *Wiley Interdisc. Rev.-Comput. Mol. Sci.* **2011**, *1*, 487−508.
(8) Wheland, G. W. *J. Am. Chem. Soc.* **1942**, *64*, 900−908.
(9) Muller, N.; Pickett, L. W.; Mulliken, R. S. *J. Am. Chem. Soc.* **1954**, *76*, 4770−4778.
(10) Olah, G. A.; Staral, J. S.; Asencio, G.; Liang, G.; Forsyth, D. A.; Mateescu, G. D. *J. Am. Chem. Soc.* **1978**, *100*, 6299−6308.
(11) Sieber, S.; Schleyer, P. v. R.; Gauss, J. *J. Am. Chem. Soc.* **1993**, *115*, 6987−6988.
(12) Solcà, N.; Dopfer, O. *Angew. Chem., Int. Ed.* **2002**, *41*, 3628−3631.
(13) Solcà, N.; Dopfer, O. *Chem.—Eur. J.* **2003**, *9*, 3154−3161.
(14) Solcà, N.; Dopfer, O. *J. Am. Chem. Soc.* **2003**, *125*, 1421−1430.
(15) Douberly, G. E.; Ricks, A. M.; Schleyer, P. v. R.; Duncan, M. A. *J. Phys. Chem. A* **2008**, *112*, 4869−4874.
(16) Lorenz, U. J.; Solcà, N.; Lemaire, J.; Maître, P.; Dopfer, O. *Angew. Chem., Int. Ed.* **2007**, *46*, 6714−6716.
(17) Ricks, A. M.; Douberly, G. E.; Duncan, M. A. *Astrophys. J.* **2009**, *702*, 301−306.
(18) Knorke, H.; Langer, J.; Oomens, J.; Dopfer, O. *Astrophys. J. Lett.* **2009**, *706*, L66−L70.
(19) (a) Solcà, N.; Dopfer, O. *Chem. Phys. Lett.* **2001**, *342*, 191−199. (b) Solcà, N.; Dopfer, O. *J. Chem. Phys.* **2004**, *120*, 10470−10482. (c) Solcà, N.; Dopfer, O. *J. Am. Chem. Soc.* **2004**, *126*, 1716−1725.
(20) Pasker, F. M.; Solcà, N.; Dopfer, O. *J. Phys. Chem. A* **2006**, *110*, 12793−12804.
(21) Andrei, H.-S.; Solcà, N.; Dopfer, O. *ChemPhysChem* **2006**, *7*, 107−110.
(22) Oomens, J.; Meijer, G.; von Helden, G. *Int. J. Mass Spectrom.* **2006**, *249*−*250*, 199−205.
(23) Vala, M.; Szczepanski, J.; Dunbar, R. C.; Oomens, J.; Steill, J. D. *Chem. Phys. Lett.* **2009**, *473*, 43−48.
(24) Chakraborty, S.; Patzer, A.; Dopfer, O. *J. Chem. Phys.* **2010**, *133*, 044307/1−12.
(25) Gerardi, H. K.; Gardenier, G. H.; Viswanathan, U.; Auerbach, S. M.; Johnson, M. A. *Chem. Phys. Lett.* **2011**, *501*, 172−178.
(26) Lorenz, U. J.; Lemaire, J.; Maître, P.; Crestoni, M.-E.; Fornarini, S.; Dopfer, O. *Int. J. Mass Spectrom.* **2007**, *267*, 43−53.
(27) Chiang, Y.; Whipple, E. B. *J. Am. Chem. Soc.* **1963**, *85*, 2763−2767.
(28) (a) Marino, G. *Adv. Heterocycl. Chem.* **1973**, *13*, 235−314. (b) Belen'kii, L. I. Vibrational selectivity in electrophilic aromatic substitution in π-excessive heteroaromatics. *Adv. Heterocycl. Chem.* **2010**, *99*, 144−183.
(29) Houriet, R.; Schwarz, H.; Zummack, W.; Andrade, J. G.; Schleyer, P. v. R. *Nouv. J. Chem.* **1981**, *5*, 505−509.
(30) Angelini, G.; Laguzzi, G.; Sparapani, C.; Speranza, M. *J. Am. Chem. Soc.* **1984**, *106*, 37−41.
(31) Hiraoka, K.; Takimoto, H.; Yamabe, S. *J. Am. Chem. Soc.* **1987**, *109*, 7346−7352.
(32) Nguyen, V. Q.; Tureček, F. *J. Mass Spectrom.* **1996**, *31*, 1173−1184.
(33) Kabli, S.; van Beelen, E. S. E.; Ingemann, S.; Henriksen, L.; Hammerum, S. *Int. J. Mass Spectrom.* **2006**, *249*−*250*, 370−378.
(34) (a) Politzer, P.; Weinstein, H. *Tetrahedron* **1975**, *33*, 915−923. (b) Chou, D.; Weinstein, H. *Tetrahedron* **1978**, *33*, 275−286.
(35) Catalán, J.; Yáñez, M. *J. Am. Chem. Soc.* **1984**, *106*, 421−422.

(36) Nalewajski, R. F.; Koninski, M. *J. Mol. Struct. (THEOCHEM)* **1988**, *165*, 365−378.
(37) Nakajima, Y.; Sakagishi, Y.; Shiibashi, M.; Suzuki, Y.; Kato, H. *J. Mol. Struct. (THEOCHEM)* **1993**, *288*, 199−205.
(38) Galabov, B.; Ilieva, S.; Koleva, G.; Allen, W. D.; Schaefer, H. F., III; Schleyer, P. v. R. *WIREs Comput. Mol. Sci.* **2012**, DOI: 10.1002/wcms.1112.
(39) Duncan, M. A. *Int. Rev. Phys. Chem.* **2003**, *22*, 407−435.
(40) (a) Okumura, M.; Yeh, L. I.; Myers, J. D.; Lee, Y. T. *J. Chem. Phys.* **1986**, *85*, 2328−2329. (b) Okumura, M.; Yeh, L. I.; Myers, J. D.; Lee, Y. T. *J. Phys. Chem.* **1990**, *94*, 3416−3427.
(41) Ebata, T.; Fujii, A.; Mikami, N. *Intl. Rev. Phys. Chem.* **1998**, *17*, 331−361.
(42) Bieske, E. J.; Dopfer, O. *Chem. Rev.* **2000**, *100*, 3963−3998.
(43) Robertson, W. H.; Johnson, M. A. *Annu. Rev. Phys. Chem.* **2003**, *54*, 173−213.
(44) Baer, T.; Dunbar, R. C. *J. Am. Soc. Mass Spectrom.* **2010**, *21*, 681−693.
(45) Bosenberg, W. R.; Guyer, D. R. *J. Opt. Soc. Am. B* **1993**, *10*, 1716−1722.
(46) Gerhards, M.; Unterberg, C.; Gerlach, A. *Phys. Chem. Chem. Phys.* **2002**, *4*, 5563−5565.
(47) (a) Schmidt, M. W.; Baldridge, K. K.; Boatz, J. A.; Elbert, S. T.; Gordon, M. S.; Hensen, J. H.; Koseki, S.; Matsunaga, N.; Nguyen, K. A.; Su, S.; Windus, T. L.; Dupuis, M.; Montgomery, J. A. *J. Comput. Chem.* **1993**, *14*, 1347−1363. (b) Gordon, M. S.; Schmidt, M. W. In *Theory and Applications of Computational Chemistry: The First Forty Years*; Dykstra, C., Frenking, G., Kim, K., Scuseria, G., Eds.; Elsevier B. V.: Amsterdam, 2005.
(48) Mellouki, A.; Liéven, J.; Herman, M. *Chem. Phys.* **2001**, *271*, 239−266.
(49) Botschwina, P.; Oswald, R. *J. Phys. Chem. A* **2011**, *115*, 13664−13672.
(50) Cohen, A. J.; Mori-Sánchez, P.; Yang, W. *Chem. Rev.* **2012**, *112*, 289−320.
(51) (a) Gimarc, B. M. *J. Am. Chem. Soc.* **1983**, *105*, 1979−1984. (b) Ott, J. J.; Gimarc, B. M. *J. Am. Chem. Soc.* **1986**, *108*, 4304−4308. (c) cf. Dieker, J.; Fröhlich, R.; Würthwein, E. U. *Eur. J. Org. Chem.* **2006**, 5339−5356 and private communication.
(52) Chen., Z.; Wannere, C. S.; Corminboeuf, C.; Puchta, R.; Schleyer, P. v. R. *Chem. Rev.* **2005**, *105*, 3842−3888.
(53) Fallah-Bagher-Shaidaei, H.; Wannere, C. S.; Corminboeuf, C.; Puchta, R.; Schleyer, P. v. R. *Org. Lett.* **2006**, *8*, 863−866.
(54) Nyulaszi, L.; Schleyer, P. v. R. *J. Am. Chem. Soc.* **1999**, *121*, 6872−6875 and references cited therein.
(55) Tielens, A. G. G. M. *Annu. Rev. Astron. Astrophys.* **2008**, *46*, 289−337.
(56) Hudgins, D. M.; Bauschlicher, C. W., Jr.; Allamandola, L. J. *Astrophys. J.* **2005**, *632*, 316−332.